J Electr Eng Technol Vol. 9, No. 1: 205-213, 2014
http://dx.doi.org/10.5370/JEET.2014.9.1.205

ISSN(Print) 1975-0102
ISSN(Online) 2093-7423

High Performance MPPT Based on Variable Speed Generator Driven by Wind Power Generation in Battery Applications

Sutha Padmanabhan* and Kannan Kaliyappan†

Abstract - A wind generator (WG) maximum power point tracking (MPPT) system is presented here. It comprises of a variable-speed wind generator, a high-efficiency boost-type dc/dc converter and a control unit. The advantages of the aimed system are that it does not call for the knowledge of the wind speed or the optimal power characteristics and that it operates at a variable speed, thus providing high efficiency. The WG operates at variable speed and thus suffers lower stress on the shafts and gears compared to constant-speed systems. It results in a better exploitation of the available wind energy, especially in the low wind-speed range of 2.5-4.5 m/s. It does not depend on the WG wind and rotor-speed ratings or the dc/dc converter power rating. Higher reliability, lower complexity and cost, and less mechanical stress of the WG. It can be applied to battery-charging applications.

Keywords: Boost converter, Maximum power point tracking (MPPT), Microcontroller, Variable speed, Wind generator (WG).

1. Introduction

WIND GENERATORS (WGs) have been widely applied both in autonomous systems for power supplying remote loads and in grid-connected applications. Although WGs accept a lower installation cost equated to photovoltaic's, the overall system cost can be further reduced applying high-efficiency power converters, controlled such that the optimal power is assumed according to the current atmospheric conditions. The WG power production can be mechanically controlled by changing the blade pitch angle [1] However, WGs of special structure are required, which is not the usual case, especially in small-size stand-alone WG systems.

A commonly used WG control system [2-6] is shown in Fig. 1(a). This topology is based on the WG optimal power versus the rotating-speed characteristic, which is usually stored in a microcontroller memory. The WG rotating speed is evaluated; then, the optimal output power is calculated and equated to the actual WG output power. The resulting error is applied to control a power interface. In a similar version detected in [7], the WG output power is evaluated and the target rotor speed for optimal power generation is deduced from the WG optimal power versus rotor-speed characteristic. The target rotor speed is compared to the actual speed, and the error is used to control a dc/dc power converter. The control algorithm has been implemented in Lab VIEW running on a PC.

In permanent-magnet (PM) WG systems, the output current And voltage is proportional to the electromagnetic torque and rotor speed, respectively. In [8,9], the rotor speed is calculated according to the measured WG output voltage, while the optimal output current is calculated

using an approximation of the current versus the rotational-speed optimal characteristic. The error resulting from the comparison of the calculated and the actual current is used to control a dc/dc converter.

The disadvantage of all above methods is that they are based on the knowledge of the WG optimal power characteristic, which is usually not available with a high degree of accuracy and also changes with rotor aging. Another approach using a two-layer neural network [10] updates online the pre programmed WG power characteristic by perturbation of the control signals around the values provided by the power characteristic. However, under real operating conditions where the wind speed changes rapidly, the continuous neural network training required results in accuracy and control-speed reduction.

A control system based on wind-speed measurements [2] is shown in Fig. 1(b). The wind speed is measured, and the required rotor speed for maximum power generation is computed. The rotor speed is also measured and compared to the calculated optimal rotor speed, while the resulting error is used to control a power interface. Implementations of fuzzy-logic-based control systems transferring the maximum power from a wind-energy-conversion system to the utility grid or to a stand-alone system have been presented in [11-13] respectively. The controllers are based on a polynomial approximation of the optimal power versus the wind-speed characteristic of the WG.

Apart from the accuracy reduction due to the approximation of the WG characteristics, an accurate anemometer is required for the implementation of the

† Corresponding Author: Dept. of Electrical and Electronic Engineering, RVSCET, Dindigul, Tamilnadu, India. (kannankmeped@gmail.com)
* Dept. of Electrical and Electronic Engineering, University College of Engineering-Panrutti, Tamilnadu, India. (suthapadmanbhan@gmail.com)
Received: June 22, 2013; Accepted: September 5, 2013

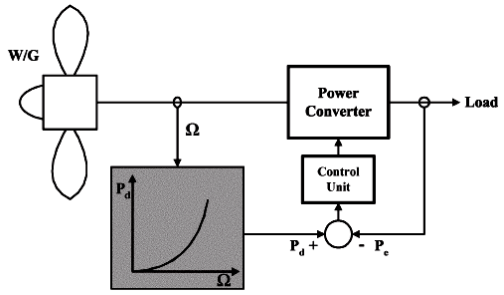

Fig. 1. Control system based on rotating speed measurements

aforementioned methods, which increases the system cost. Furthermore, due to wind gusts of low-energy profile, extra processing of wind-speed measurement must be incorporated in the control system for a reliable computation of the available wind energy, which increases the control system complexity.

1.1. Control system based on rotating-speed measurements:

WG rotating speed is measured. Optimal output power is calculated and compared to the actual output power. Resulting error is used to control a power interface. WG output power is measured.

1.2. Control system based on output power measurements:

Target rotor speed for optimal power generation is derived from the WG optimal power versus rotor-speed characteristic. Target rotor speed is compared to the actual speed. Resulting error is used to control a dc/dc power converter.

1.3 Control system based on wind speed measurements:

Wind speed is measured. Required rotor speed for maximum power generation is computed. Rotor speed is measured and compared to the calculated optimal rotor speed. Resulting error is used to control a power interface. Require knowledge of the WG optimal power characteristics, which is not available with a high degree of accuracy and also changes with ageing. Less efficiency, under real operating conditions where, the wind speed changes rapidly. Use of anemometer increases the system cost. For low-energy wind gusts, extra processing of wind-speed measurements must be incorporated in the control system for a reliable computation of the available wind energy, which increases its complexity.

The incoming wind energy is converted to mechanical energy and then to three-phase ac electricity by the wind turbine and generator. The dc is converted to ac by the three-phase bridge rectifier. The dc voltage level is boosted

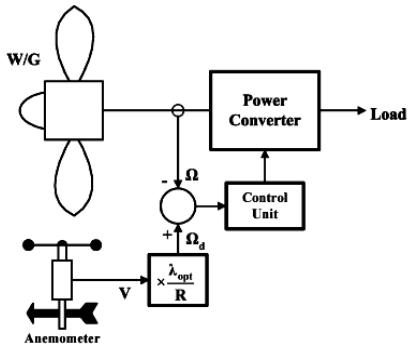

Fig. 2. Control system based on wind speed measurements

by the boost-type dc/dc converter. The MPPT circuit is used to extract maximum power from the wind by monitoring the WG output power using measurements of the WG output voltage and current and directly adjusting the dc/dc converter duty cycle according to the result of comparison between successive WG-output-power values The WG operates at variable speed and thus suffers lower stress on the shafts and gears compared to constant-speed systems. It results in a better exploitation of the available wind energy, especially in the low wind-speed range of *2.5-4.5 m/s*. It does not depend on the WG wind and rotor-speed ratings or the dc/dc converter power rating higher reliability, lower complexity and cost, and less mechanical stress of the WG. This paper is organized as follows. The WG characteristics are described in Section II, the proposed system is analyzed in Section III, and the theoretical and experimental results are Presented in Section IV.

2. Wind Turbine Modelling System

The tip speed ratio λ is defined as:

$$\lambda = \frac{\omega R}{v} \tag{1}$$

Where, ω, R and V represent turbine rotational speed, Turbine blade radius and the wind velocity respectively.

In general, the power captured from the wind turbine can be written as:

$$P_m = C_p(\lambda, \beta)\rho \frac{A}{2} v^3 \tag{2}$$

where *Cp* (λ , β) is the power coefficient, ρ is the air density, *V* is the wind speed, *R* is the blade radius, β is the blade pitch angle and λ is the tip speed ratio. The power curve speeds of a typical wind turbine are shown in Fig. 3. The value of maximum wind turbine output power per unit can be obtained by putting zero pitch angle and Betz limit,

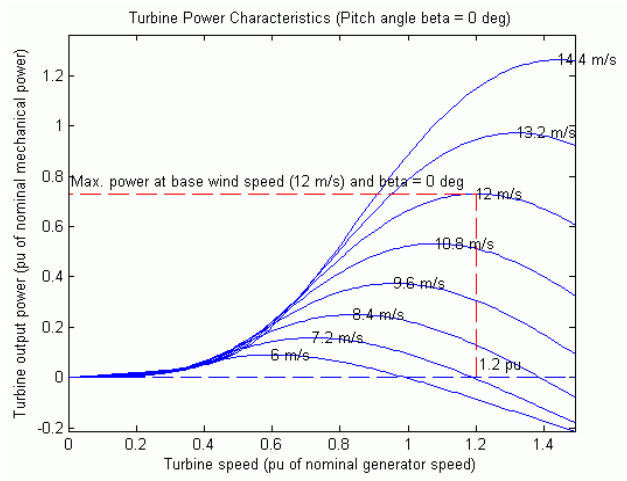

Fig.3. Turbine Output Characteristics (Zero Pitch angle)

when the velocity of wind turbine is 12 m/s.

It is not suitable for real time application. In this proposed paper, maximum power can be captured in different wind turbine speeds. Considering the generator efficiency ηG, the total power produced by the WG P is

$$P = \eta G P_m \tag{3}$$

The WG power coefficient is maximized for a tip-speed ratio Value *o*pt when the blades pitch angle is $\beta = 0\circ$. The WG power curves for various wind speeds are shown in Fig. 3. It is observed that, for each wind speed, there exists a specific Point in the WG output power versus rotating-speed characteristic where the output power is maximized. The control of the WG load results in a variable-speed WG operation, such that maximum power is extracted continuously from the wind (MPPT control). The value of the tip-speed ratio is constant for all maximum power points (MPPs), while the WG speed of rotation is related to the wind speed as follows:

$$\Omega_n = \lambda_{opt} \frac{V_n}{R} \tag{4}$$

Where Ω_n is the optimal WG speed of rotation at a wind Velocity V_n . Besides the optimal energy production capability, another advantage of variable-speed operation is the reduction of stress on the WG shafts and gears, since the blades absorb the wind torque peaks during the changes of the WG speed of rotation. The disadvantage of variable-speed operation is that a power conditioner must be employed to play the role of the WG apparent load. However, the evolution of power electronics helps reduce the power-converter cost and increases its reliability, while the higher cost is balanced by the energy production gain. The torque curves of the WG, consisting of the interconnected wind-turbine/generator system, for various generator output voltage levels under various wind speeds,

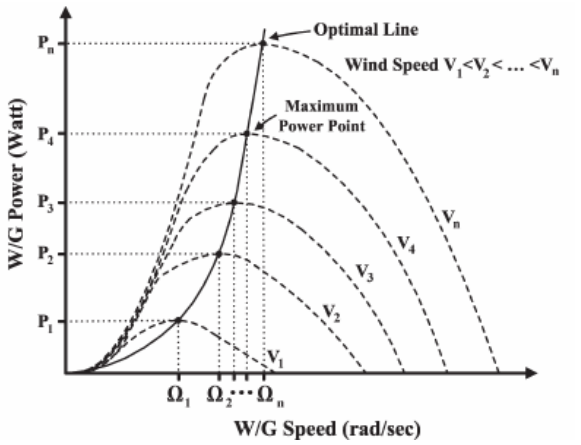

Fig.4. WG Power curves at various wind speeds

are shown in Fig. 4. The generator is designed such that it operates in the approximately linear region corresponding to the straight portion of the generator torque curves in Fig. 4, under any wind-speed condition.

3. Proposed System

3.1 MPPT algorithm

As mentioned in Section of Fig. 5, the MPPT process in the proposed system is based on directly adjusting the dc/dc converter duty cycle according to the result of the comparison of successive WG-output-power measurements. Although the wind speed varies highly with time, the power absorbed by the WG varies relatively slowly, because of the slow dynamic response of the interconnected wind-turbine/generator system. Thus, the problem of maximizing the WG output power using the converter duty cycle as a control variable can be effectively solved using the steepest ascent method according to the following control law: Wherever Times is specified, Times Roman or Times New Roman may be used. If neither is available on your word processor, please use the font closest in appearance to Times. Avoid using bit-mapped fonts. True Type 1 or Open Type fonts are required. Please embed all fonts, in particular symbol fonts, as well, for math, etc.

$$D_k = D_{k-1} + C_1 \frac{\Delta P_{k-1}}{\Delta D_{k-1}} \tag{5}$$

Where D_k and D_k-1 are the duty-cycle values at iterations k and $k-1$, respectively ($0 < D_k < 1$); $\Delta Pk-1/\Delta D_k-1$ is the WG power gradient at step $k-1$; and $C1$ is the step change. In order to ensure that this method results in convergence to the WG MPP at any wind-speed level, it is adequate to prove that the function P (D), relating the WG power P and the dc/dc converter duty cycle D, has a single extreme point coinciding with the WG MPPs depicted in

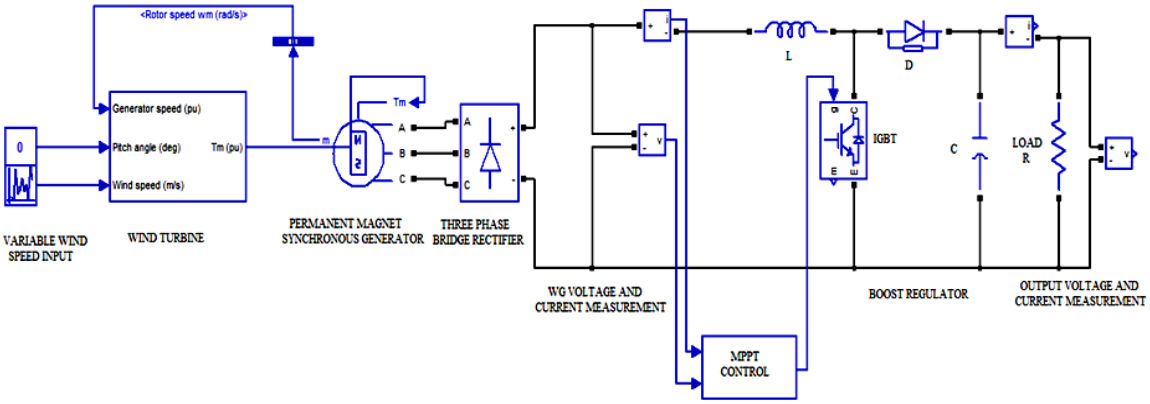

Fig. 5. Block diagram of proposed system

Fig. 3. Considering the WG power characteristics depicted in Fig. 3, it is obvious that at the points of maximum power production

$$\frac{dP}{d\Omega} = 0 \tag{6}$$

where Ω is the WG rotor speed.

Applying the chain rule, the above equation can be written as:

$$\frac{dP}{d\Omega} = \frac{dP}{dD} \cdot \frac{dD}{dV_{WG}} \cdot \frac{dV_{WG}}{d\Omega_e} \cdot \frac{d\Omega_e}{d\Omega} = 0 \tag{7}$$

Where V_{WG} is the rectifier output voltage level and Ω_e is the generator-phase-voltage angular speed. In case of a buck-type dc/dc converter, its input voltage is related to the output (battery) voltage and the duty cycle

as follows:

$$D = \frac{V_O}{V_{WG}}$$
$$\frac{dD}{dV_{WG}} = -\frac{1}{V^2_{WG}} V_O \neq 0 \tag{8}$$

where V_o is the battery voltage level.

The wind-turbine rotor speed is related to the generator speed

as follows:

$$\Omega_e = P.\Omega$$
$$\frac{d\Omega_e}{d\Omega} = P > 0 \tag{9}$$

where p is the generator number of pole pairs.

The rectifier output voltage V_{WG} is proportional to the generator phase voltage V_{ph}; considering Fig. 4, it is concluded that

$$\frac{dV_{PH}}{d\Omega_e} > 0 \tag{10}$$

And

$$\frac{dV_{WG}}{d\Omega_e} = 0 \tag{11}$$

Considering (7)-(11), it holds that

$$\frac{dP}{d\Omega} = 0 \Leftrightarrow \frac{dP}{dD} = 0 \tag{12}$$

Thus, the function $P(D)$ has a single extreme point, coinciding with the WG MPP, and the dc/dc converter duty-cycle adjustment according to the control law of (5) ensures convergence to the WG MPP under any wind-speed condition.

The power maximization process is shown in Fig. 6. Since the duty-cycle adjustment follows the direction of *dP/dD*, the duty-cycle value is increased in the high-speed side of the WG characteristic, resulting in a WG-rotor-speed reduction and power increase, until the MPP is reached. Similarly when the starting point is in the low-speed side, following the direction of *dP/dD* results in duty-cycle reduction and the subsequent convergence at the MPP, since the WG rotor speed is progressively increased. The proposed method can also be applied to maximize the output power of the WG in case of alternative dc/dc

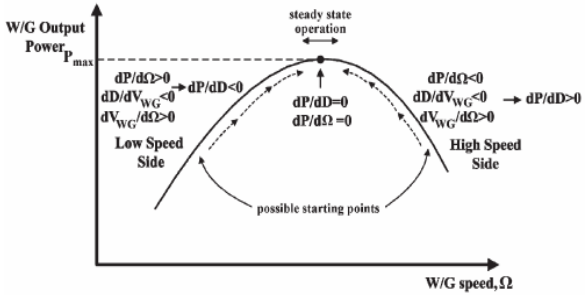

Fig. 6. Mppt Tracking Process diagram

converter configurations.

1) Boost converter:

$$V_{WG} = (1-D)V_O, dV_{WG}/dD = V_o \neq 0.$$

2) Buck-boost converter:

$$V_{WG} = V_o(1-D)/D, dV_{WG}/dD = -(1/D^2)V_o \neq 0.$$

3) Cuk converter:

$$V_{WG} = V_o(1-D)/D, dV_{WG}/dD = -(1/D^2)V_o \neq 0.$$

4) Flyback converter:

$$V_{WG} = V_o(1-D)/D, dV_{WG}/dD = -(1/D^2)V_o \neq 0.$$

In order to reduce the impact of the sensor accuracy on the Generated power, the control law of (5) has been implemented based on incremental WG power measurements, rather than absolute measurements, as follows:

$$D_k = D_{k-1} + \Delta D_{k-1}$$
$$\Delta D_{k-1} = C_2.sign(\Delta D_{k-2}).sign(P_{in,k-1} - P_{in,k-2}) \quad (13)$$

where ΔD_{k-1} is the duty-cycle change at step $k - 1$; $P_{in,k-1}$ and $P_{in,k-2}$ are the converter input-power levels at steps k - 1 and $k - 2$, respectively; C_2 is a constant determining the speed and accuracy of the convergence to the MPP; and the function sign(x) is defined as

$$sign(x) = 1, \quad if, x \geq 0$$
$$sign(x) = -1 \quad if, x \prec 0 \quad (14)$$

3.2 Power-electronic interface

The detailed diagram of the proposed system is depicted in Fig. 6. The WG ac output voltage is first converted to dc form using a three-phase full-wave bridge rectifier. The rectifier output capacitor value *C*r is calculated as follows:

$$C_r \geq \frac{1}{12fR_L}\left(1 + \frac{1}{\sqrt{2}RF}\right) \quad (15)$$

Where R_L is the WG load resistance, f is the WG output voltage frequency, and RF is the rectifier output voltage ripple factor. A buck-type dc/dc converter is used to convert the high dc input voltage to the 24-V battery voltage level. The fly back Diode D is of fast-switching type, while four power MOSFETs are connected in parallel, to comply with the converter power capability requirements. A power MOSFET is used to switch on and off a 10-Ω resistive dummy load, thus limiting the WG speed of rotation under severe conditions. The power inductor L and the input and output capacitor values, C_{in} and C, respectively, are calculated as follows [14, 15]

$$L \geq \frac{V_{om}(1-D_{cm})}{f_s|\Delta I_{LM}|} \quad (16)$$

$$C \geq \frac{1}{8}\frac{(1-D_{cm})}{Lf_sRF_o} \quad (17)$$

$$C_{in} \geq \frac{1}{8}\frac{(1-D_{cm})I_{om}D_{cm}}{RF_{in}V_{WGm}f_s} \quad (18)$$

Where f_s is the dc/dc converter switching frequency, D_{cm} is the duty cycle at maximum output power of the converter, ΔI_{Lm} is the peak-to-peak ripple of the inductor current, V_{om} is the maximum of the dc component of the output voltage, I_{om} is the dc component of the output current at maximum output power, RF_o is the output voltage ripple factor (typically $RF_o \leq 2\%$), RF_{in} is the input voltage ripple factor (typically $RF_{in} \leq 2\%$), and V_{WGm} is the converter input voltage at maximum power.

The control unit is supplied by the battery and consists of an Intel 80C196KC microcontroller unit with an external erasable programmable ROM (EPROM) and a static RAM (SRAM), the interface circuits comprising of sensors and amplifiers connected to the on-chip A/D converter, as well as the power MOSFET IC drivers. A 39.2-kHz 8-bit-resolution on chip pulse width modulation (PWM) output is used to control the power MOSFETs of the buck converter through the IR2104 driver IC, while an I/O port pin controls the power MOSFET that switches the dummy load through the IR2121 driver IC. Another I/O port is used to drive a liquid crystal display (LCD) showing various parameters of the system operation.

The WG and battery voltages are measured by means of voltage dividers interfaced to operational-amplifier (op-amp) - based voltage-follower circuits. The dc/dc converter input current is equal to the average value of the power MOSFET current, which has a pulse-type waveform and is measured with a unidirectional current transformer.

The flowchart of the control algorithm is shown in Fig. 7. The battery voltage is monitored and when it reaches a predefined set point, the MPPT operation is suspended in order to protect the battery stack from overcharging. The PWM duty-cycle value is stored in an 8-bit register of the microcontroller, taking values that correspond to duty-cycle values 0% - 99.6%. The WG output power is calculated and compared to the WG output power at the previous iteration of the algorithm. According to the result of the comparison, the sign of the duty-cycle change ΔD is either complemented or remains unchanged. Subsequently, the PWM output duty cycle is changed appropriately, thus implementing the control law described by (13).

After the duty-cycle regulation, the WG voltage is checked; if it is higher than the maximum preset limit, the dummy load is connected to the dc/dc converter input in order to protect the Fig. 7. MPPT process algorithm. WG

from over speeding. The dummy load is disconnected when the WG output voltage falls below the lower preset limit. They hysteresis introduced by the maximum and minimum preset limits is necessary to avoid the dummy load continuous on/off switching.

4. Theoretical and Experimental Results

The prototype MPPT system was developed based on the Method described above [16-20] The WG used in the experiments has A three-phase output rated at 100-V rms thus, the dummy-load Connection and disconnection voltage levels are set at 140 and 100 V, respectively. The dc/dc converter was designed according to the methodology analyzed in Section III. The power switch consists of four MOSFETs rated at 200 V and 30 an each, while the fly back diode has a 200-ns reverse-recovery time. The calculated input and output capacitor values are 470 and 4700 μF, respectively. The output inductor value is 45 μH and is wound on a Siemens E65/21 ferrite core with a 3-mm air gap. The converter operates in continuous conduction mode, and the switching frequency is proximately 40 kHz. The dc input voltage value in this case is VWG = 66.8 V, and the dc output voltage value is VO = 33.9 V. Such a high value of the output (battery) voltage

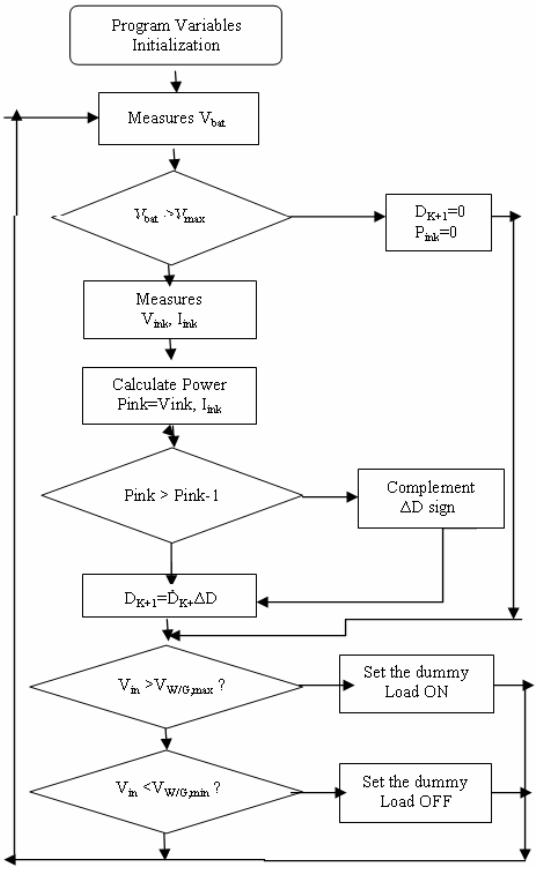

Fig. 7. MPPT Process Algorithm

appears in case that the battery is fully charged and a sudden increase of the converter input power follows. If this is the case, the MPPT process is suspended according to the MPPT algorithm flowchart shown in Fig. 7. The dc/dc converter efficiency is defined as

$$\eta = \frac{P_o}{P_{in}} = \frac{P_o}{P_o + P_d} \tag{19}$$

Where Pin and Po are the dc/dc converter input and output power, respectively, and Pd is the power loss consisting of the MOSFET and diode conduction and switching losses, the inductor core and copper losses, and the control system power Consumption.

The theoretical values were calculated using data given by the manufacturers of the circuit elements. It is observed that the efficiency is quite high and relatively constant for a wide output power range. This is important in WG systems since the generated power depends strongly on the atmospheric conditions and varies over a wide range. The wind speed, the WG output power, and the corresponding rotor speed of rotation, measured during a 22-min time period and sampled with a 0.1-Hz rate, are depicted in Fig. 10. It is observed that the WG power production follows the changes of the wind speed. In order to further evaluate the MPPT performance, the wind speed, the WG power, and the WG rotational speed were measured during a 4-h test period with a 0.1-Hz sampling rate. The measured WG rotational-speed range was divided in intervals of 10-r/min width each, and the ensemble average (Pi,Ωi) of the WG power and rotational-speed measurements corresponding to each interval was calculated as follows [2]:

$$P_i = \frac{1}{n_i}\sum_{j_1}^{n_i} P_{ij} \tag{20}$$

$$\Omega_i = \frac{1}{n_i}\sum_{j_1}^{n_i} \Omega_{ij} \tag{21}$$

Where Ωij is the j^{th} rotational-speed measurement in the i^{th} Interval, P_{ij} is the j^{th} power measurement in the interval, i^{th} And n_i is the number of data sets in the ith interval. The resulting ensemble averages (Pi,Ωi) were used to build the diagram shown in Fig. 11. It can be concluded that, using the proposed MPPT method, the output power follows the optimal power versus the rotational-speed characteristic. The maximum deviation from the optimal line is approximately 7%, mainly due to a lower number of measurements in the power range of 400-600 W, while a 30% of this deviation is attributed to the rectifier power loss. For comparison purposes, the output power of a WG directly connected to a 24-V battery through a rectifier is also indicated in the figure. The power produced in that case is much lower compared to that with the proposed MPPT method. For a further investigation of

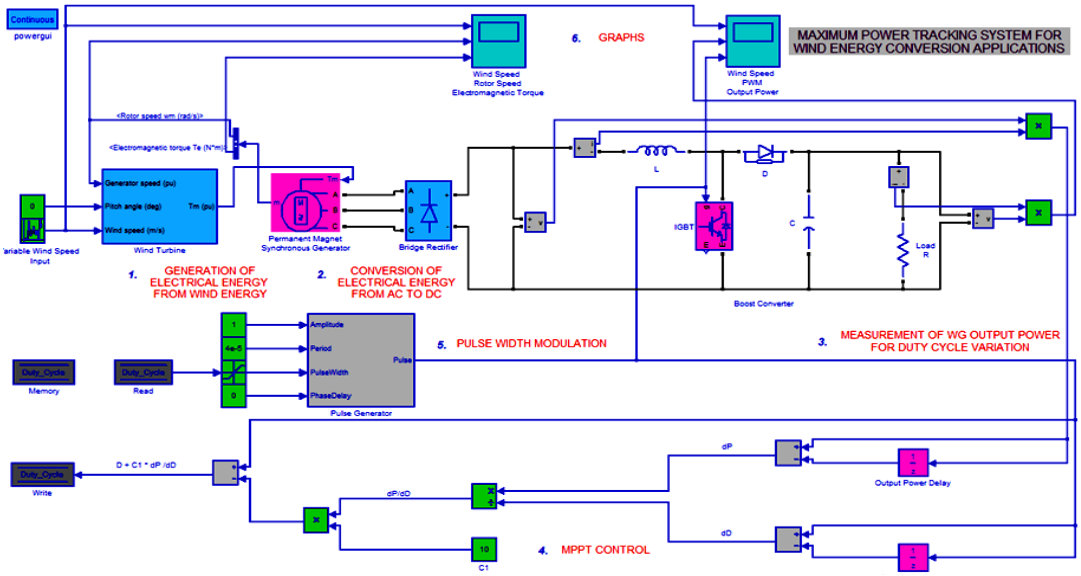

Fig. 8. Simulation of a proposed system

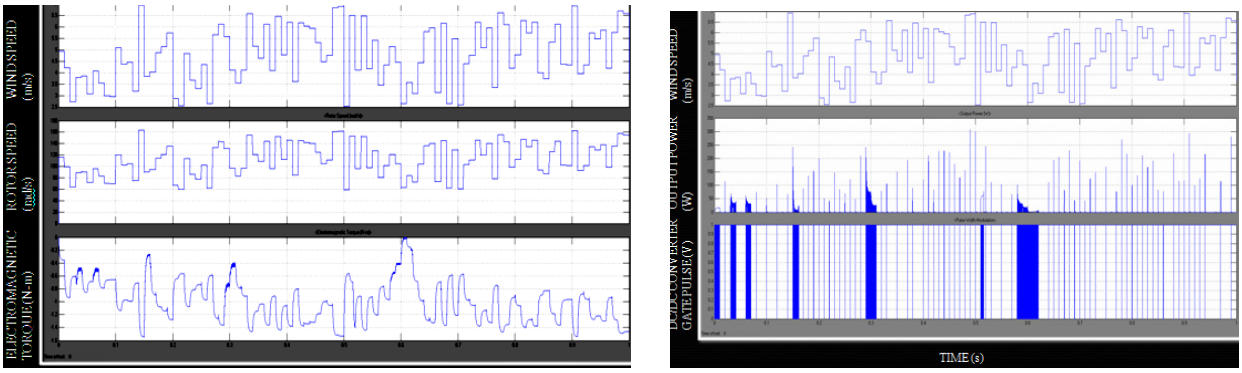

(a) (b)

Fig. 9. (a), (b) Simulation of proposed system results

the WG-output-power behaviour at various wind-speed levels, the measured wind-speed range was divided in intervals each of 1-m/s width. The ensemble average (P_k , V_k) of the WG power and wind-speed measurements corresponding to each interval is calculated as follows:

$$P_k = \frac{1}{n_k}\sum_{p=1}^{n_k} P_{kp} \tag{22}$$

$$V_k = \frac{1}{n_k}\sum_{p=1}^{n_k} V_{kp} \tag{23}$$

Where V_{kp} is the pth wind-speed point in the kth interval, P_{kp} is the pth power point in the kth interval, and n_k is the number of data sets in the kth interval. The proposed MPPT algorithm is modeled and simulated the wind turbine model is built from the SIMULINK library in Fig.8. The theoretical and measured efficiency for various output power levels is shown in Fig. 9(a, b).

The switching frequency was chosen to be *25* MHz. It was seen that the duty-cycle of the gate pulse of the dc/dc converter varied with the variation in the wind speed. Thus, maximum power was continuously extracted from the wind and the efficiency increased. The experimental hardware with the control setup of high performance based MPPT drive circuit is shown in Figs. 10 and 11.

It is noticed that the WG output power follows the optimal WG power versus wind-speed characteristic with a maximum deviation of approximately 6.5%, while the rectifier power loss is responsible for 30% of this deviation. The power production of a WG directly connected to a battery-rectifier load is also indicated in the same figure. The WG-output-power benefit using the proposed MPPT method compared to the battery-rectifier configuration is 11%-50% in the power range of 100-600 W. the Fig. 12. is clearly concluded that the proposed method results in a better exploitation of the available wind energy, especially in the low wind-speed range of 2.5-4.5 m/s.

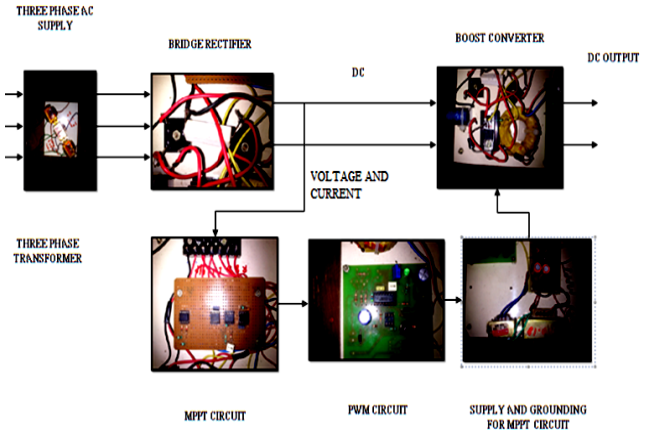

Fig. 10. Block diagram of proposed hardware system module

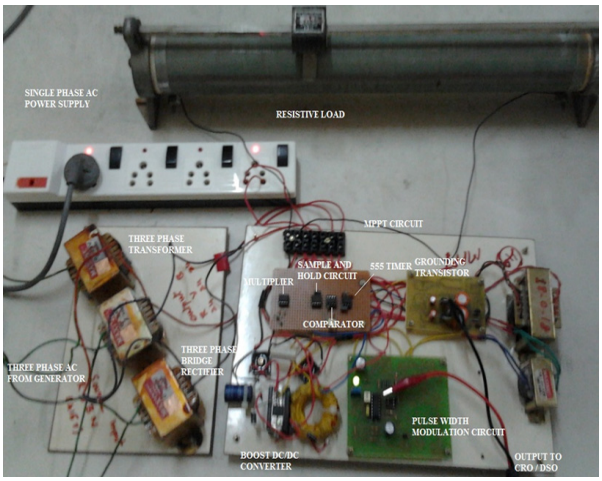

Fig.11. Boost chopper based hardware system module

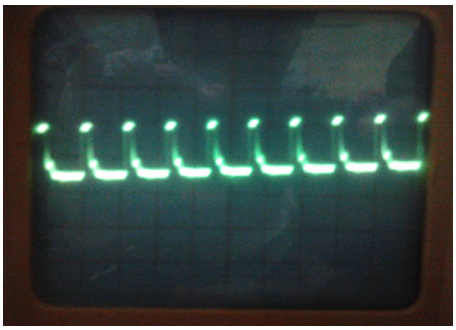

Fig.12. Boost chopper based hardware system results

The power transferred to the battery bank is derived consider in the dc/dc converter efficiency, the WG output power, and the power loss. The use of the proposed method improves the power transferred to the battery by 7%-45% in the power range of 100-600 W, compared to the simple battery-rectifier configuration. The experimental results of the past-proposed WG MPPT methods either have been obtained with laboratory-built WG simulators, thus the MPPT performance under real conditions has not been exhibited, or their performance has not been adequately investigated so as to indicate the deviation from the optimal power production.

4.1. Abbreviations

Where,

ρ - air density, in kg/m^3
β - pitch angle, in *degrees*
V - wind speed, in *m/s*
R - blade radius, in *m*
A - rotor-swept area, in m^2
Ω - WG rotor speed, in *rad/s*
η_G - generator efficiency

5. Conclusion

In this paper, the development of a novel WG maximum power tracking control system is presented, comprising of a high-efficiency boost-type dc/dc converter and a microcontroller-based control unit. The advantages of the proposed MPPT method are as follows: 1) no knowledge of the WG optimal power characteristic or measurement of the wind speed is required and 2) the WG operates at variable speed and thus suffering lower stress on the shafts and gears compared to constant-speed systems. The proposed MPPT method does not depend on the WG wind and rotor-speed ratings or the dc/dc converter power rating. Experimental results of the proposed system indicate that the WG output power is increased by 11%-50%, compared to the case where the WG is directly connected via a rectifier to the battery bank. The proposed method results in a better exploitation of the available wind energy, especially in the low wind-speed range of 2.5-4.5 m/s, where the power production of the battery-rectifier configuration is relatively low. The proposed method can be easily extended to include battery charging management or additional RES control, while it can also be modified to control a dc/ac converter in the case of a grid-connected wind-energy-conversion system.

The laboratory results from the implementation of the simple high performance based MPPT Control algorithm indicate that the proposed system has advantages. These include high reliability, cost effectiveness, and a wide speed range for variable-speed wind-turbine controllers.

References

[1] N. Kodama, T. Matsuzaka, and N. Inomata, "Power variation control of a wind turbine generator using probabilistic optimal control, including feed forward control from wind speed," *Wind Eng.,* vol. 24, no. 1, pp. 13-23, Jan. 2000.

[2] L. L. Freris, *Wind Energy Conversion Systems. Englewood Cliffs, NJ: Prentice-Hall,* 1990, pp. 182-184.
[3] Rashid, Muhammad H. (2011), *Power electronics, circuits, devices, and applications, 3rd ed., Pearson Education,* New Delhi, India.
[4] V. Valtchev, A. Bossche, J. Ghijselen, and J. Melkebeek "Autonomous renewable energy conversion system," *Renew. Energy*, vol. 19, no. 1, pp. 259-275, Jan. 2000.
[5] A. Miller, E. Muljadi, and D. S. Zinger, "A variable speed wind turbine power control," *IEEE Trans. Energy Conversion,* vol. 12, pp. 181-187, June 1997.
[6] E. Muljadi and C. P. Butterfield, "Pitch-controlled variable-speed wind turbine generation," *IEEE Trans. Ind. Appl.*, vol. 37, no. 1, pp. 240-246, Jan. 2001.
[7] A. M. De Broe, S. Drouilhet, and V. Gevorgian, "A peak power tracker for small wind turbines in battery charging applications," *IEEE Trans. Energy Convers.,* vol. 14, no. 4, pp. 1630-1635, Dec. 1999.
[8] O. Honorati, G. Lo Bianco, F. Mezzetti, and L. Solero, "Power electronic interface for combined wind/PV isolated generating systems,". *in Proceedings of. Eur. Union Wind Energy Conf.,* Göteborg, Sweden, 1996, pp. 321-324.
[9] G. Lo Bianco, O. Honorati, and F. Mezzetti, "Small-size stand alone wind energy conversion system for battery-charging," *in Proceedings of. 31st Universities Power Engineering Conf.*, Iráklion, Greece, 1996, pp. 62-65.
[10] R. Spee, S. Bhowmik, and J. Enslin, "Novel control strategies for variable speed doubly fed wind power generation systems," *Renew. Energy,* vol. 6, no. 8, pp. 907-915, Nov. 1995.
[11] M. G. Simoes, B. K. Bose, and R. J. Spiegel, "Design and performance evaluation of a fuzzy-logic-based variable-speed wind generation system*," IEEE Trans. Ind. Applicant.*, vol. 33, pp. 956-965, July/Aug, 1997.
[12] A. Z. Mohamed, M. N. Eskander, and F. A. Ghali, "Fuzzy logic control based maximum power tracking of a wind energy system," *Renew. Energy*, vol. 23, no. 2, pp. 235-245, Jun. 2001.
[13] R. M. Hilloowala and A. M. Sharaf, "A rule-based fuzzy logic controller for a PWM inverter in a standalone wind energy conversion scheme," *IEEE Trans. Ind. Appl.*, vol. 32, no. 1, pp. 57-65, Jan./Feb. 1996.
[14] N. Mohan, T. Undeland, and W. Robbins, *Power Electronics: Converters, Applications and Design*, 2nd Ed. New York: Wiley, 1995, pp. 164-172.
[15] Hui, Joanne (Dec. 2008), "An adaptive control algorithm for maximum power point tracking for wind energy conversion systems", *M.S.(Engg.) thesis,* Queen's University, Kingston, Ontario, Canada.
[16] Analog Devices Inc. (2012), Data sheet, *AD633*.
[17] National Semiconductor Corporation (2000), Data sheet, *LF398*.
[18] National Semiconductor Corporation (2006), Data sheet, *LM555*.
[19] Motorola Inc. (1996), Data sheet, *LM358*.
[20] Texas Instruments Inc. (2003), Data sheet, *SG3524*.

S.Sutha received B.E from Government College of Engg. Tirunelveli, Monomania Sundarar University in 1996, M.E. from College of Engg. Guindy, Anna University Chennai in 2000 and Ph.D. from Anna University Chennai in 2008. Presently, she is working as Assistant Professor of ANNA UNIVERSITY (Panruti Campus) Tamil Nadu, India.

K.Kannan, received B.E course from R.V.S College of Engineering and Technology in 2006, M.E[PED] from Sri Venkateshwara College of Engineering Sriperumbhdur in 2009. Now, Research Scholar of Anna University and presently working as Assistant Professor in Department of Electrical and Electronics Engineering in R.V.S College of Engineering and Technology, Dindigul, Tamil Nadu, India.